Journal of Nano- and Electronic Physics
Vol. 18 No 3, 03020(5pp) (2026)

Журнал нано- та електронної фізики
Том 18 № 3, 03020(5cc) (2026)

REGULAR ARTICLE

OPEN ACCESS

Frequency-Selective Surface (FSS) Exhibiting High Angular Stability and Polarization-Insensitive Characteristics for Wideband Applications

Anitha Bondalapati, Bappadittya Roy*

School of Electronics Engineering, VIT-AP University, 522237 Inavolu, India

(Received 07 March 2026; revised manuscript received 20 June 2026; published online 26 June 2026)

A wideband polarization-insensitive, and angularly stable frequency selective surface (FSS) is proposed in this work. The designed unit cell consists of two octagonal rings connected to each other with splits along their sides. The structure is designed on a low-loss FR-4 dielectric substrate with a thickness of 1.6 mm, and the unit-cell footprint measures 10 × 10 mm². The proposed FSS achieves a wide transmission band from 4.9 GHz to 11.5 GHz, providing approximately 6.6 GHz of usable bandwidth with the operating frequency of 5.8 GHz. This range covers several practical applications, including C-band (4-8 GHz), wireless local area networks (WLAN) at 5.2 GHz and 5.8 GHz, WiMAX and various filtering and radar applications. Furthermore, FSS arrays of sizes 2 × 2, 3 × 3, and 4 × 4 were analyzed, and their simulated responses were evaluated. And finally, the frequency selective surface with 4 × 4 array is subsequently developed and fabricated on an FR-4 substrate. The simulated results proved that the proposed FSS is polarization-insensitive for various oblique incident angles and maintains angular stability up to 70° for varying polarization angles, with measured results showing good agreement with the simulations. The compact geometry and ease of fabrication make the structure appropriate for incorporation into modern communication platforms.

Keywords: C-band, FR-4, Frequency selective surface (FSS), Radar communications, Wide band, WLAN, WiMAX applications.

DOI: 10.21272/jnep.18(3).03020 PACS number: 84.40.Ba

1. INTRODUCTION

Frequency-selective surfaces (FSSs) have been thoroughly researched for their ability to provide various applications, such as randoms, reflectors, absorbers, and spatial filtering of electromagnetic waves, which possess bandpass or bandstop characteristics with optimal unit-cell geometries and periodic configurations [1]. A structure consisting of unit cells has been proposed to enhance bandwidth, angular stability, downsizing, and multiband functionality. Dual-layer methodologies, exemplified by the square-loop topology developed by equivalent circuit modeling in [2], have exhibited enhanced wideband rejection. A compact triple band-stop FSS designed for sub-6-GHz applications, effectively spanning NR n39/n40, LTE 42/43, and LTE 46 bands with robust angular stability, was documented in [3]. Reconfigurable systems have evolved, such as the PIN-diode-loaded square-loop FSS in [4], which offers adjustable band stop characteristics and phase modulation. Second-order band stop design was developed within the millimeter-wave spectrum, resulting in band rejection and angular stability up to 60°, as referenced in [5]. Graphene-based metasurfaces in the terahertz region have features of polarization-insensitivity and absorption being researched to maintain steady angular performance at oblique incidences up to 50° [6].

FSSs can also be used for security applications and health protection, represented by the penta-bandstop surface in [7], which decisively reduces undesired frequencies. Further contributions encompass ultra-wide stopband FSS attaining significant attenuation levels [8], dual-bandstop configurations obtained from super formula loops exhibiting stable angular response stability up to 60° [9], and highly compact L-band FSSs facilitating polarization-independent functionality [10]. Further contributions include dual-band 5G FR2 FSS featuring rotational symmetry for both TE and TM stability [11], angularly stable single-layer bandstop FSSs tailored for X-/Ku-band applications [12], and ENG-based miniaturized bandstop filters demonstrating extensive rejection bandwidths and negative-index properties over a 220-MHz range [13]. A highly angular-stable dual-band stop FSS operating in the C- and X-bands was proposed in [14] for suppressing satellite downlink frequencies. The structure exhibits a negative refractive index over a 220 MHz range, and tunable multi-zero FSSs facilitate adaptable stopband regulation with a stable response to 40° [15].

In this work implementing the compact, single layered FSS achieving the polarization insensitive features with the wideband rejection with excellent angular stability maintain a simple geometry fabrication on the low-cost FR-4 substrate with substrate height 1.6 mm. Achieving the better performance by reducing the design complexity like adding of passive components (PIN diodes) and multiple layers.

* bappadittya.roy@vitap.ac.in

Cite this article as: A. Bondalapati et al., *J. Nano- Electron. Phys.* 18 No 3, 03020 (2026) https://doi.org/10.21272/jnep.18(3).03020

2. PROPOSED UNITCELL DESIGN

The design steps and geometric characteristics of the proposed unit cell are illustrated in Fig. 1. This structure is developed FR-4 substrate with height of the substrate 1.6 mm, a dielectric constant (ε_r) of 4.4, and a loss tangent of 0.02. the length of the unitcell should be less than $\lambda/2$[1]. The overall size of the unit cell is $0.91\lambda_0 \times 0.91\lambda_0$ with the operating frequency 5.8 GHz. All the simulations are performed using HFSS tool.

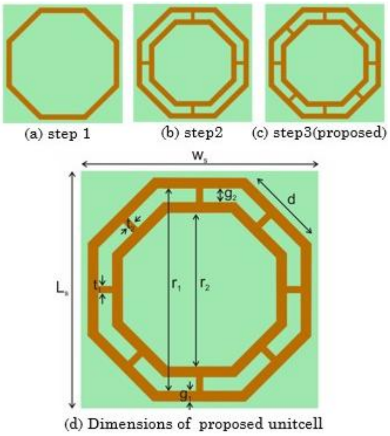

Fig. 1 – Evolution of the proposed unit-cell structure(a)-(c) and (d) final unit-cell geometry with design parameters

Initially, only one octagonal loop is designed on the substrate, which results in a single resonance in the S_{21} response, indicating its bandstop behavior. In the subsequent step, an additional concentric octagonal loop is introduced inside the original loop. Both loops are interconnected through short splits located along the four sides, improving electromagnetic coupling and consequently broadening the S_{21} bandwidth. Finally, supplementary diagonal splits are incorporated to enhance the effective inductance–capacitance (LC) characteristics and confine surface currents along the loops. This modification results in a well-defined bandstop response with a pronounced S_{21} attenuation peak. Table 1 summarizes the detailed dimensions of the proposed unit cell.

Table 1 – Geometrical parameters of the unit cell

Parameter	Value (mm)	Parameter	Value (mm)
W_s	10	g_2	0.55
L_s	10	t_1	0.3
r_1	8.5	t_2	0.3
r_2	6.45	d	2.7
g_1	0.45		

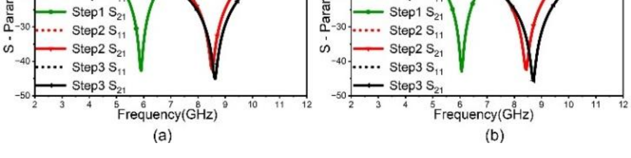

Fig. 2 – Simulated reflection (S_{11}) and transmission (S_{21}) coefficients of the unit-cell structure for the three design steps under (a) TE and (b) TM polarization

Fig. 2 illustrates the reflection and transmission coefficients of the unit cell at various design steps under both TE and TM modes. The simulations are carried out using Floquet ports and periodic boundary conditions. In Step 1, the S_{21} response exhibits a bandwidth from 4.07 GHz to 7.70 GHz in TE mode and from 4.19 GHz to 7.89 GHz in TM mode. In Step 2, with the better electromagnetic coupling between the loops the bandwidth got increased to 5.60 GHz-10.89 GHz in TE mode and 5.55 GHz-10.83 GHz in TM mode . In Step 3 makes the coupling even stronger, which improves the bandwidth to 4.91 GHz-11.58 GHz in TE mode and 4.90 GHz-11.75 GHz in TM mode. The peak S_{21} attenuation is – 45 dB. The transmission coefficient (S_{21}) confirms the bandstop characteristics of the proposed unit cell, where as the reflection coefficient(S_{11}) remains close to 0 dB, indicating that most of the incident power is reflected rather than transmitted.

Fig. 3 displays the surface current distribution of the proposed unit cell, demonstrating significant current confinement along both the inner and outer octagonal loops, especially at the split gaps and coupling portions. This confirms that the proposed design consistently produces an effective bandstop resonance.

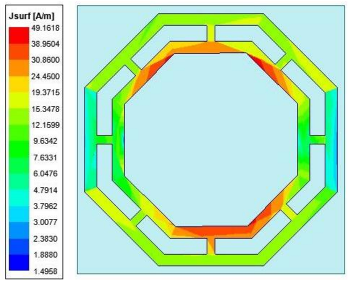

Fig. 3 – Surface current distribution of the proposed unit cell at the resonant frequency

3. PARAMETRIC INVESTIGATION

Fig. 4 illustrates the parametric study of four important design parameters and their impact on the transmission coefficient of the unit cell. Figure 4(a) demonstrates the impact of altering the metallic strip width (g_1), which directly influences the current path length and the effective inductance of the configuration. A noticeable frequency shift is observed as c increases.

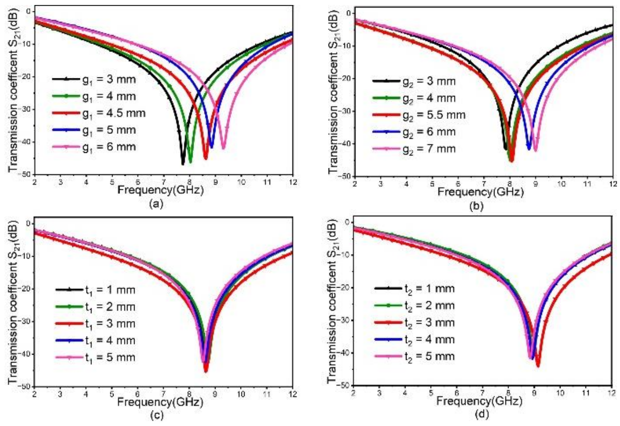

Fig. 4 – Parametric analysis of the proposed unit cell, influencing on the S_{21}: (a) Loop width (g_1), (b) gap between loops (g_2), (c) edge split width (t_1), and (d) diagonal split width(t_2)

The width $g_1 = 4.5$ mm is chosen as it generates the optimal bandwidth, ranging from 5.54 GHz to 11.08 GHz.

Fig. 4(b) examines the separation gap (g_2) between the two octagonal loops. This parameter determines the coupling strength between the loops. A very small gap results in excessively strong coupling, increased losses, and reduced stopband depth. An optimal intermediate value of g_2 as 5.5 mm yields a peak S_{21} attenuation of − 43 dB. From Fig. 4(c), the effect of varying the split-width parameter (t_1) is analyzed. Minimal changes in frequency are noted; still, $t_1 = 3$ mm offers an extensive operational stopband from 4.91 GHz to 11.42 GHz, rendering it the optimal choice.

Finally, Fig. 4(d) shows the influence of parameter d. Small variations in d affect the depth of the stopband. The value $t_2 = 3$ mm is chosen, as it produces a slightly deeper S_{21} notch of approximately − 45 dB. Based on these parametric observations, the optimal values of g_1, g_2, t_1 and t_2 are selected, and the final design of the proposed unit cell is established.

4. PROPOSED FSS DESIGN

Frequency-selective surfaces (FSSs) are inherently periodic structures. Fig. 5(a) shows the FSS configuration formed using a 2 × 2 array (four unit cells) to approximate the behavior of an infinite periodic surface. The overall size of this array is 20 × 20 mm², and it exhibits an S_{21} attenuation of approximately − 35 dB along with its corresponding bandwidth. When the number of unit cells is increased to a 3 × 3 array (30 × 30 mm²), the structure more closely emulates an infinite periodic surface (Fig. 5(b)).

However, noticeable variations in bandwidth are observed when comparing the single unit cell, the 2 × 2 array, and the 3 × 3 array. This is because the single unit cell is simulated under ideal infinite periodic boundary conditions and is not affected by external disturbances. In contrast, the 2 × 2 and 3 × 3 arrays experience mutual coupling among adjacent cells and finite-size edge effects, which influence the overall bandwidth response.

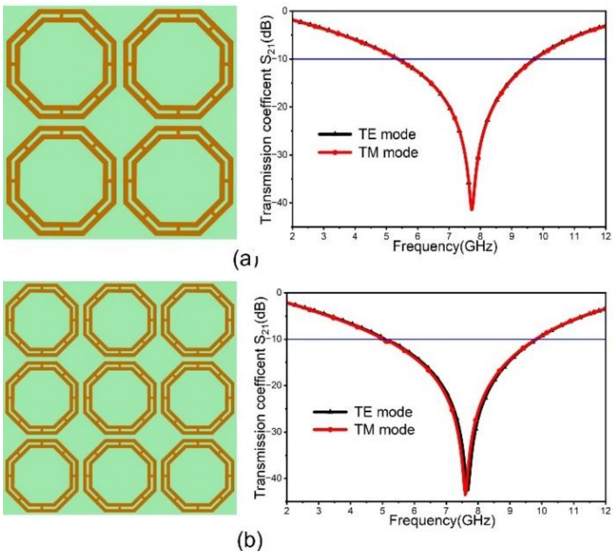

Fig. 5 – Periodic arrangement and S_{21} response for TE and TM modes of finite FSS arrays: (a) 2 × 2 and (b) 3 × 3

A finalized FSS with a 4 × 4 periodic arrangement is subsequently simulated, fabricated, and experimentally characterized. The fabricated prototype has physical dimensions of 40 × 40 mm², with an inter-element spacing of 0.6 mm between adjacent unit cells. The structure is realized on an FR-4 substrate, and the corresponding fabricated sample is shown in the Fig. 6.

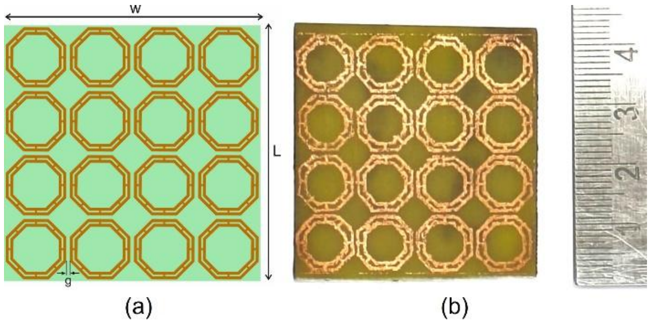

Fig. 6 – (a), Geometry of the finalized 4 × 4 FSS array, where $W = L = 40$ mm and $g = 0.6$ mm and (b) Fabricated prototype

5. RESULTS AND DISCUSSION

For an FSS, polarization insensitivity and angular stability are critical performance requirements, and these can be evaluated by varying both the incident angle and the polarization state of the incoming electromagnetic wave.

Fig. 7 exhibits the transmission coefficient (S_{21}) of the suggested frequency selective surface (FSS) for transverse electric (TE) and transverse magnetic (TM) polarizations at azimuth angles from $\varphi = 0°$ to 60°.

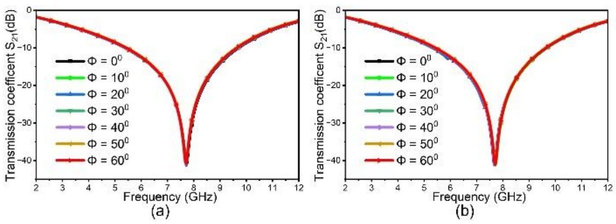

Fig. 7 – Transmission coefficient S_{21} response for various polarization angle (φ) (a) TE mode and (b) TM mode

The results demonstrate that the TE and TM responses nearly overlap at all angles of incidence. This stable response verifies that the designed FSS is insensitive to polarization and preserves its filtering performance over a broad span of varies angles.

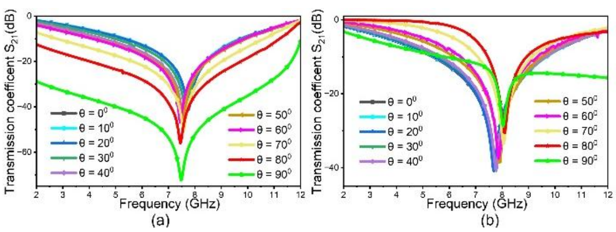

Fig. 8 – Transmission coefficient S_{21} response for various incidence angles under (a) TE mode and (b) TM mode

The transmission coefficent response of the suggested FSS for varying incidence angles (Elevation angles) θ from 0° to 90° is shown in Fig. 8. From plot the

S_{21} curves for both TE and TM modes remain nearly same, indicating the stable stopband behavior. A minor shift appears for angles above 70° beacause of the stronge tangential field components at near-grazing incidence in free space. Overall, the results indicate that the FSS retains good angular stability up to about 60°.

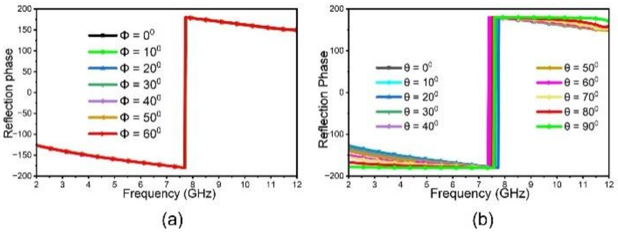

Fig. 9 – Reflection phase(S_{11}) characteristics of the proposed FSS by varying angles: (a) polarization angles (φ) and (b) incidence angles (θ)

The reflection phase characteristics of the proposed FSS are shown in Fig. 9. The results shows a phase reversal of approximately 180°. The reflective phase response remains almost identical for variations in the azimuth angle φ, representing the strong polarization insensitivity behavior. Furthermore, the phase remains stable for incidence angles up to 70°, resulting in satisfactory angular stability. The continuous phase behavior across angular and polarization variations provides good interference when the FSS operating as a reflector alongside with an antenna, thereby helpful for potential gain improvement.

The surface current distribution of the 4 × 4 FSS array at the resonant frequency is presented in Fig. 10. It shows strong current around the loops, with high concentrations of flow at the corners and at coupling regions. The uniform current distribution at the edge is very less. The well spread and uniform resonant behavior justifies the noticeable stopband seen in the transmission characteristics and enhances the stable, polarization-insensitive performance of the designed FSS. Table 2 shows the comparative analysis of the proposed work with the existing designs as the proposed design exhibits the compact size with featuring both polarization insensitive and angularly stable behavior.

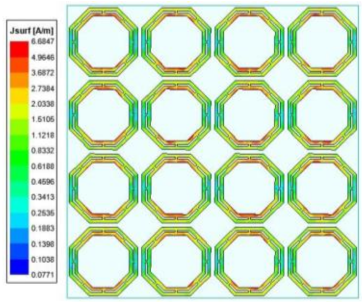

Fig. 10 – Surface current distribution of the finalized 4 × 4 FSS

Table 2 – Comparative analysis with existing FSS structures

Ref. No	Substrate	Dimensions (mm²)	Operating Frequency (GHz)	Polarization insensitive	Angular stability
[9]	FR-4	$0.11\lambda_0 \times 0.11\lambda_0$	5.6	Yes	0°-60°
[10]	FR-4	$0.034\lambda_0 \times 0.034\lambda_0$	1.6	Yes	0°-60°
[11]	RT5880	$0.7\lambda_0 \times 0.7\lambda_0$	24.78	Yes	–
[12]	FR-4	$0.25\lambda_0 \times 0.25\lambda_0$	10	No	0°-60°
[13]	Taconic RF-35	$0.125\lambda_0 \times 0.125\lambda_0$	3.96	Yes	0°-45°
[14]	FR-4	$0.138\lambda_0 \times 0.138\lambda_0$	3.7	No	0°-85°
[15]	Rogers4350B	$0.145\lambda_0 \times 0.145\lambda_0$	4	No	0°-40°
Proposed work	FR-4	$0.91\lambda_0 \times 0.91\lambda_0$	5.8	Yes	0°-70°

6. CONCLUSION

The work represents that the suggested dual octagonal ring FSS design exhibits a compact and accurate wideband response with band stop characteristics, which is more suitable for the modern RF and electromagnetic filtering applications. With the integration of the concentric loops and strategically placed splits, the proposed FSS achieves strong current confinement, which results in a broad operating band from 4.9 to 11.5 GHz. The frequencies in this range are used for several critical applications, including C-band, WLAN (5.2/5.8 GHz), WiMAX, short-range sensing, and X-band radar systems. In addition, the FSS has a stable performance for varying incidence angles up to 70° and is polarization insensitive, making the designed structure suitable for environmental changes where signal orientation and incidence direction vary. With all these features, the proposed FSS is suitable for integration into randoms, electromagnetic shielding panels, antenna sub-systems, and spatial filtering layers used in broadband wireless and radar infrastructures.

ACKNOWLEDGEMENT

The authors extend their gratitude to the Department of SENSE at VIT-AP University, RGEMS, and V-Launch Projects for their invaluable support and encouragement throughout the course of this research

REFERENCES

1. W. Afzal, M.Z. Baig, A. Ebrahimi, M.R. Robel, M.T.A. Rana, W. Rowe, *Telecom* **5** No 4, 1102 (2024) https://doi.org/10.3390/telecom5040056.
2. N. Liu, D. Guo, Xianjun Sheng, Jingjing Fan, C. Zhang, *IEEE Antennas Wireless Propag. Lett.* **16**, 2721 (2017) https://doi.org/10.1109/LAWP.2017.2743114.
3. S. Panchal, M.N. Kumar, S.H.S., P.K. Sahu, M.I. Abdullah, J. Malik, D.V.S.R. Varma, U. Singh, A. Bhowmik, A.J. Santhosh, *Res. Eng.* **27**, 106495 (2025) https://doi.org/10.1016/j.rineng.2025.106495.
4. Patrick Danuor, Young-Bae Jung, Jung-Ick Moon, Jung-Nam Lee, *IEEE Antennas Wireless Propag. Lett.* **24** No 1, 172 (2024) https://doi.org/10.1109/LAWP.2024.3487842.
5. Soumik Dey, Sukomal Dey, Shiban K. Koul, *IEEE Trans. Antennas Propag.* **70** No 8, 7282 (2022) https://doi.org/10.1109/TAP.2022.3145457.
6. Subbarao Genikala, Anumoy Ghosh, Pratik Mondal, Bappadittya Roy, *Plasmonics* **20**, 5991 (2025) https://doi.org/10.1007/s11468-025-03043-y.
7. Sanjeev Yadav, C.P. Jain, M.M. Sharma, *IEEE Trans. Electromagn. Compat.* **61** No 3, 887 (2018) https://doi.org/10.1109/TEMC.2018.2839707.
8. Gouri Shankar Paul, Kaushik Mandal, Ali Lalbakhsh, *AEU – Int. J. Electron. Commun.* **132**, 153630 (2021) https://doi.org/10.1016/j.aeue.2021.153630.
9. S. Khajevandi, Homayoon Oraizi, Poordaraee, *IEEE Antennas Wireless Propag. Lett.* **17** No 5, 731 (2018) https://doi.org/10.1109/LAWP.2018.2812698.
10. Sayi Soundariya Sampath, S. Ramprabhu, J. Jegadish, *IEEE Trans. Electromagn. Compat.* **61** No 5, 1678 (2018) https://doi.org/10.1109/TEMC.2018.2869664.
11. Sibel Ünaldı, Nigar Berna Teşneli, *Optik – International Journal for Light and Electron Optics* **315**, 172040 (2024) https://doi.org/10.1016/j.ijleo.2024.172040.
12. Saeed Abbasi, Javad Nourinia, Changiz Ghobadi, Mohsen Karamirad, and Bahman Mohammadi, *AEU – Int. J. Electron. Commun.* **89**, 85 (2018) https://doi.org/10.1016/j.aeue.2018.03.018.
13. Sourodipto Das, Anil Rajput, Biswajeet Mukherjee, *IEEE Lett. Electromagn. Compat. Pract. Appl.* **6** No 1, 11 (2023) https://doi.org/10.1109/LEMCPA.2023.3327027.
14. Gundu Venkatesh, Muthiah Thottappan, S.P. Singh, *IEEE Trans. Electromagn. Compat.* **64** No 6, 2055 (2022) https://doi.org/10.1109/TEMC.2022.3200212.
15. Yuhong Ma, Ye Yuan, Dehua Wang, Qingzhan Shi, Naichang Yuan, *IEEE Access* **7**, 156536 (2019) https://doi.org/10.1109/ACCESS.2019.2947310.

Частотно-селективна поверхня (FSS) з високою кутовою стабільністю та нечутливими до поляризації характеристиками для широкосмугових застосувань

Anitha Bondalapati, Bappadittya Roy

School of Electronics Engineering, VIT-AP University, 522237 Inavolu, India

Запропоновано широкосмугову поляризаційно-нечутливу та кутово-стабільну частотно-селективну поверхню (ЧСП). Розроблена елементарна комірка складається з двох восьмикутних кілець, з'єднаних одне з одним з розрізами вздовж їхніх боків. Структура розроблена на діелектричній підкладці FR-4 з низькими втратами товщиною 1,6 мм, а площа елементарної комірки становить 10 × 10 мм². Запропонована ЧСП досягає широкої смуги передачі від 4,9 ГГц до 11,5 ГГц, забезпечуючи приблизно 6,6 ГГц корисної пропускної здатності з робочою частотою 5,8 ГГц. Цей діапазон охоплює кілька практичних застосувань, включаючи C-діапазон (4-8 ГГц), бездротові локальні мережі (WLAN) на частотах 5,2 ГГц та 5,8 ГГц, WiMAX та різні застосування для фільтрації та радіолокації. Крім того, було проаналізовано масиви ЧСП розміром 2 × 2, 3 × 3 та 4 × 4, а також оцінено їх змодельовані відгуки. І, нарешті, частотно-селективна поверхня з масивом 4 × 4 згодом розроблена та виготовлена на підкладці FR-4. Результати моделювання довели, що запропонований FSS є поляризаційно нечутливим для різних кутів падіння під кутом та зберігає кутову стабільність до 70° для різних кутів поляризації, причому виміряні результати добре узгоджуються з результатами моделювання. Компактна геометрія та простота виготовлення роблять структуру придатною для інтеграції в сучасні комунікаційні платформи.

Ключові слова: C-діапазон, FR-4, Частотно-селективна поверхня (FSS), Радіолокаційний зв'язок, Широкосмуговий зв'язок, WLAN, Застосування WiMAX.